IL NUOVO CIMENTO Vol. 36 C, N. 2 Marzo-Aprile 2013
DOI 10.1393/ncc/i2013-11516-4

Colloquia: Nanoforum 2012

Nanoparticle dynamics in the presence and absence of a cellular uptake altering chemical

A. M. Schrand(1)(2)(*), J. B. Lin(2), C. M. Garrett(2), S. V. Brownheim(3), S. M. Hussain(2)(**), F. Cubadda(4)(***), A. R. M. Nabiul Afrooz(5) and N. B. Saleh(5)

(1) *Munitions Directorate, Air Force Research Laboratory - Eglin Air Force Base FL 32542, USA*
(2) *Applied Biotechnology Branch, Human Effectiveness Directorate, Air Force Research Laboratory - Wright Patterson Air Force Base, OH 45433-5707, USA*
(3) *Air Force Institute of Technology (AFIT) - Wright Patterson Air Force Base OH 45433-5707, USA*
(4) *Department of Food Safety and Veterinary Public Health, Istituto Superiore di Sanità Viale Regina Elena 299, 00161 Rome, Italy*
(5) *Civil and Environmental Engineering, University of South Carolina 300 Main Street, Columbia, SC 29208, USA*

ricevuto il 26 Aprile 2013

Summary. — The far-reaching applications of nanoparticles (NPs) in drug delivery, medical imaging, diagnostics, and therapeutics have led to an increased potential for interfacing with a diverse range of biological environments. While metallic NPs such as copper NPs have been explored for their antimicrobial and catalytic properties, they have been shown to induce undesirable toxic effects. Nonetheless, biomodulators may be employed to control this cytotoxicity. Dynasore is a dynamin GTPase inhibitor that has been shown to rapidly and reversibly block clathrin-dependent endocytic traffic within minutes of application. Here, we demonstrate that Dynasore can chemically bio-modulate the toxic effects of copper nanoparticles (Cu NPs), but not through reducing Cu NP internalization. In fact, Dynasore seems to possess secondary effects that have been unreported to date. We propose and test three potential mechanisms of cytotoxicity modulation: 1) through changes in agglomeration pattern, 2) through potential quenching of reactive oxygen species (ROS), and 3) through Cu^{+2} ion chelation. These results have far-reaching implications for understanding the complex interactions that occur at the interface of NPs in biological environments, especially during mechanistic chemical modification strategies.

PACS 87.85.Rs – Nanotechnologies-applications.
PACS 47.63.-b – Biological fluid dynamics.
PACS 87.85.Ng – Biological signal processing.
PACS 82.39.-k – Chemical kinetics in biological systems.

(*) E-mail: amanda.schrand@eglin.af.mil
(**) E-mail: saber.hussain@wpafb.af.mil
(***) E-mail: francesco.cubadda@iss.it

1. – Introduction

The far-reaching applications of nanoparticles (NPs) in drug delivery, medical imaging, diagnostics, and therapeutics have led to an increased potential for interfacing with a diverse range of biological environments. Copper NPs (Cu NPs) specifically have been implicated for their novel antimicrobial applications as biocides, antibiotic treatment alternatives, and nanocomposite coatings [1, 2]. However, as recently reviewed, metallic NPs composed of transition metals like Cu may contribute to adverse health conditions including concentration-dependent alterations in critical physiological processes due to improper intracellular trafficking, accumulation to cytotoxic concentrations, and generation of reactive oxygen species (ROS) [3]. The relationship between NP physiochemical properties, uptake, and toxicity is based upon complex interactions, *e.g.*, aggregation, dissolution, that occur in the biological milieu. For instance, the introduction of chemicals to block endocytosis, or other internalization pathways of NPs, may have additional unforeseen biological consequences on their cytotoxicity.

One such endocytosis inhibitor is the dynamin GTPase inhibitor Dynasore, a small molecule commonly utilized to rapidly and reversibly block cellular uptake [4-6]. Dynasore functions by inhibiting dynamin, a protein required for clathrin-dependent vesicle formation [4, 7] and has been utilized in a variety of cell lines at concentrations ranging from 10 μM to 100 μM and for fairly short exposure times ranging from 5 min to 6 h [4, 7-11]. We previously utilized Dynasore to elucidate the temporal and mechanistic uptake of biocompatible, fluorescent nanodiamonds into cells [12]. Other groups have demonstrated the ability of Dynasore to block the internalization of Zn(II)-phthalocyanine-containing liposomes [11], polystyrene NPs [10], and D-penicillamine–coated quantum dots [13]. Moreover, other groups have used Dynasore to elucidate the mechanisms by which polystyrene NPs traffic across Madin-Darby canine kidney cell II monolayers [14] and to reveal that the internalization of polystyrene NPs differs in primary cell lines *versus* related tumor cell lines [15]. Minor cytotoxic effects are sometimes observed at higher doses of Dynasore over longer periods of time as this chemical inhibitor may participate in a chemical reaction or begin to affect normal cellular trafficking.

In this study, murine neuroblastoma (N2A) cells were pretreated with 25 μM Dynasore for 1 h followed by 3 h of exposure to two different sizes of Cu NPs. The pretreatment methodology was a critical component of the rescue effect, which is consistent with other studies using endocytosis inhibitors [4, 7-11]. Here, we present a novel side-effect of Dynasore pretreatment that aids in rescuing cell viability following exposure to toxic Cu NPs, independent of its effects on uptake and the primary size of the particle.

2. – Materials and methods

2˙1. *Copper samples.* – The particulate copper samples consisted of small metallic Cu nanoparticles (Cu 90, $\sim$ 80–90 nm, American Elements, 99% metals basis, PN: CU-M-02M-NP.025N) and large metallic Cu nanoparticles (Cu 480, $\sim$ 500 nm, American Elements, 99% metals basis, PN: CU-M-02-MP.01UM). The soluble salt form of copper was copper (II) chloride dehydrate, purchased from Sigma Aldrich (C3279).

2˙2. *Nanoparticle characterization.*

2˙2.1. Transmission Electron Microscopy (TEM). Copper nanoparticles (Cu NPs) were dispersed in water and drop-cast onto formvar-carbon–coated TEM grids, then imaged with a Philips/FEI CM200 TEM at 200 kV. Final bright-field TEM (BF-TEM) images were obtained with Revolution software and saved as tiff images. Analysis of ap-

proximately one hundred individual Cu NPs from each sample yielded average sizes of 88±30 nm for Cu 90 and 477±184 nm for Cu 480. Therefore, based upon these values, the Cu NP samples —although fairly polydisperse in size— were appropriately categorized as either small (∼ 90 nm) or large (∼ 480 nm).

2˙2.2. Powder X-ray Diffraction (XRD). Copper nanoparticles (Cu NPs) were sprinkled onto slides coated with silicone grease prior to analysis on a Rigaku 2500 X-ray diffraction unit. All of the data was acquired under the following parameters: divergence slit = scatter slit = 1 deg, divergence height limiting slit = 10 mm, receiving slit = 0.6 mm. Powders were scanned in theta-2 theta geometry (also known as Bragg-Brentano geometry) from 2 theta 20 deg to 100 deg. The sampling interval was 0.05 deg, and the scan speed was 3 deg per minute with continuous scan. The power parameters were 50 KV, 300 mA, so 15 KW.

2˙2.3. Dynamic Light Scattering (DLS). Particle solutions were prepared and analyzed as previously described [16]. Briefly, Cu particles were suspended in DMEM/F12 cell culture media at a final concentration of 50 μg/mL and immediately analyzed for initial agglomerate sizes (0 h). Then, the samples were incubated at 37 °C for 3 h to observe alterations in agglomerate size in solution.

2˙2.4. Nanoparticle size measurements. Average particle size measurement and particle size distribution of the Cu 90 and Cu 480 nanoparticles in cell culture media was determined using ALV-CGS 3 compact goniometer system (ALV-GmbH, Langen, Germany), equipped with a 22 mW, 632.8 nm He-Ne laser and coupled with ALV/LSE-5004 digital auto correlator (ALV-GmbH, Langen, Germany). Approximately 2 mL of a 25 mg/L nanoparticle solution in DMEM/F12+1% streptomycin was added into previously cleaned disposable borosilicate glass vials (Fisher Scientific, Pittsburg, PA). The cleaning procedure is described elsewhere [17]. Scattered light intensity was measured at 37 °C by a photon counting module (Perkin Elmer, Dumberry, Canada) operating at 1.2 A and 5 V. The scattering angle of 90° was used for 1 h, with a 15 s time interval between consecutive readings. The scattering intensity was interpreted as hydrodynamic radius using second order cumulant analysis [18]. A similar procedure was followed to perform DLS measurements of Cu NPs in presence of Dynasore with DMEM/F12+1% streptomycin.

2˙2.5. Acellular ROS. In order to measure the amount of ROS generated by Cu NPs independently of the cellular system, an acellular ROS was performed as described in Braydich-Stolle *et al.* [19]. The ROS probe was made by deacetylating the 2′, 7′-dichlorofluorescein diacetate (DCFH-DA) probe in NaOH. Immediately prior to analysis, horseradish peroxidase (HRP) reagent was added to the DCFH-DA solution. To measure ROS, the DCFH-HRP probe was added to different concentrations of nanoparticles in cell culture media and incubated at 37 °C for 30 min.

2˙3. *Cell culture and related experiments.*

2˙3.1. Cell culture. Neuroblastoma (N2A) cells were purchased from ATCC (Neuro-2a line, CCL-131) and grown in an atmosphere of 5% CO_2 at 37 °C. Growth media for the neuroblastoma cells was DMEM/F12 supplemented with 10% normal fetal bovine serum (FBS) and 1% Pencillin-streptomyocin (ATCC). Other cell culture supplies included 10× Phosphate buffered saline (pH 7.4) and 2.5% trypsin (Gibco Invitrogen^{TM} Corporation, Carlsbad, CA).

2˙3.2. Endocytosis inhibitor Dynasore. Murine neuroblastoma (N2A) cells were pretreated with 25 μM Dynasore for 1 h, followed by 3 h of exposure to Cu NPs. This concentration was chosen based on literature values and control experiments (data not shown).

2˙3.3. MTS assay for mitochondrial function. The 3-(4,5-dimethylthiazol-2-yl)-5-(3-carboxymethoxyphenyl)-2-(4-sulfophenyl)-2H-tetrazolium (MTS) assay assesses cellular viability based on mitochondrial function. After 1 h of incubation with MTS, a dark purple color developed within the cells, indicating the formation of a water-soluble formazan product by active mitochondria in live cells. The formazan product was quantified with a microplate reader at 490 nm. A reading from 0 min was subtracted out of the final reading to account for background absorbance due to the NPs or the solution. The percent reduction of MTS was compared to controls (cells not exposed to particles), which represented 100% MTS reduction.

2˙3.4. Cellular Reactive Oxygen Species (ROS). The generation of intracellular reactive oxygen species (ROS) was determined using the fluorescent probe 2,7-dichlorohydrofluorescein diacetate (DCHF-DA) under a light controlled environment as described by Wang and Joseph [20], with minor modifications as previously described by Hussain and Frazier [21]. The reactivity of the DCFH probe was evaluated with the positive control, hydrogen peroxide, by serial dilutions of stock 30% H_2O_2 (Sigma) in dosing media.

2˙3.5. Cellular uptake of copper particles with TEM. N2A cells were processed for TEM according to Schrand *et al.* [22]. Briefly, the cells were seeded in T-75 flasks and, at 85% confluency, incubated with 25 μg/mL of the Cu NPs with or without 25 μM Dynasore pretreatment. Three hours later, the cells were fixed in 2% paraformaldehyde/2.5% glutaraldehyde in PBS for 2 h. Thereafter, the cells were post-fixed with 1% osmium tetroxide for 1 h and then scraped from the plate and centrifuged. The cells were dehydrated using increasing concentrations of ethanol with three changes of 100% ethanol. The samples were then placed in 100% LR White resin and cured overnight at 60 °C in BEEM® capsules. The samples were thin-sectioned on a Leica Ultracut ultramicrotome at a thickness of ∼100 nm and imaged using a Philips/FEI CM200 TEM at 200 kV.

2˙3.6. Atomic absorption spectroscopy for quantification of Cu uptake. Approximately 2×10^6 cells were seeded in T-75 cell culture flasks and exposed to Cu particles. The samples were washed, centrifuged and counted on a haemocytometer prior to acid digestion and dilution. The samples were analyzed on a Varian AA240 atomic absorption spectrometer for total amount of copper in a standardized 5–10 mL sample, and the data was collected as micrograms/milliliter (equivalent to parts per million) with atomic absorption spectroscopy (AAS).

2˙3.7. Inductively Coupled Plasma - Mass Spectroscopy (ICP-MS) for ionic dissolution. Characterization of ionic release from Cu NPs was performed after filtration with MicroKros hollow fiber membranes from Spectrum Laboratories, Inc. The pore rating used was 10 kDa to ensure only ions could pass through the membrane. The fibers were rinsed with ethanol to produce a hydrophilic surface, and then rinsed with water thoroughly to remove all trace amounts of alcohol. After the preparation of the filter, the solutions were passed through the fibers repeatedly to remove the disassociated ions. ICP-MS was conducted to obtain ionic concentrations. Samples were diluted in 1% nitric acid prior to running on a Perkin Elmer Elan DRC-e ICP-MS. The DRC gas was methane at 0.55 mL/min.

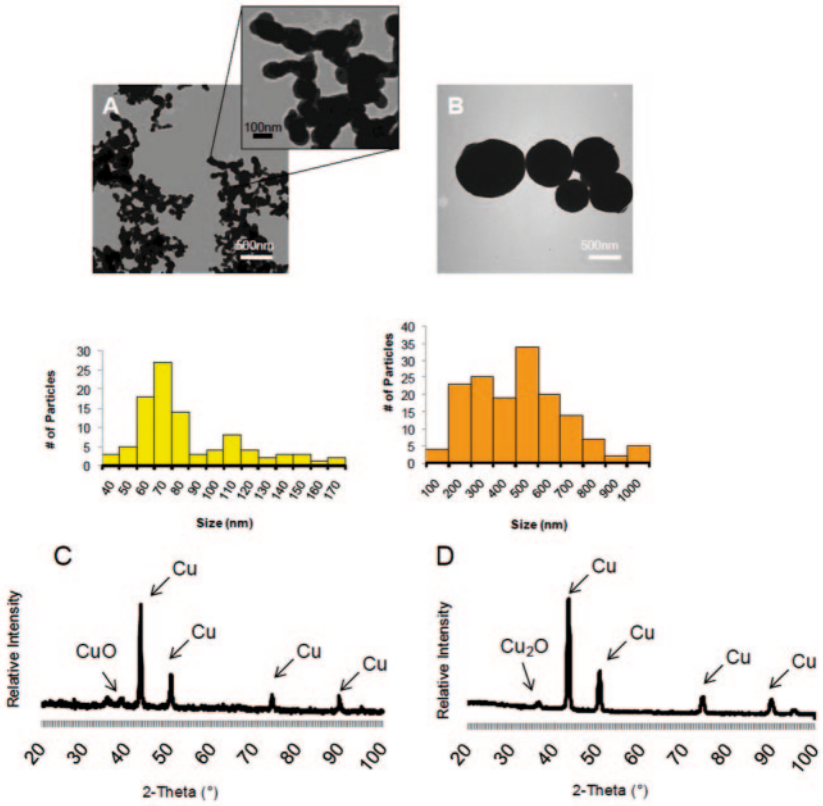

Fig. 1. – Characterization of Cu NPs. (A-B) Bright field transmission electron micrographs and associated size distributions of Cu NPs. (A) Cu 90 with average diameter of 88 ± 30 nm and (B) Cu 480 with average size of 477 ± 184 nm. Inset in (A) shows details of surface morphology compared to original image, which was taken at the same magnification to demonstrate the size difference between samples. (C-D) Powder X-ray diffraction (XRD) patterns demonstrating negligible amounts of surface oxidation in both the (C) Cu 90 and the (D) Cu 480.

2˙3.8. High-Performance Liquid Chromatography (HPLC). Solutions were prepared and incubated at 5% CO_2 and 37 °C in dosing media to simulate the potential reaction conditions during chemical bio-modulation. Samples were analyzed using Zorbax XDB-C18 columns and the Agilent 1100 series liquid chromatography system coupled with UV detection. The mobile phases were A) water with 0.1% Trifluoro acetic acid (TFA) and B) 100% methanol with 0.1% TFA, with an initial concentration of 100% A increasing up to 100% B in 40 min. Detection was carried out with UV at 254 nm.

3. – Results and discussion

Copper samples were first characterized to understand the role of size and aggregation behavior on cellular end points of viability, oxidative stress, and uptake. Transmission electron micrographs (TEM) reveal small and large Cu NPs with an average size of $\sim$ 90 nm (88 ± 30 nm, Cu 90, fig. 1A) and $\sim$ 480 nm (477 ± 184 nm, Cu 480, fig. 1B), respectively. The Cu 480 displayed a more homogenous spherical morphology compared

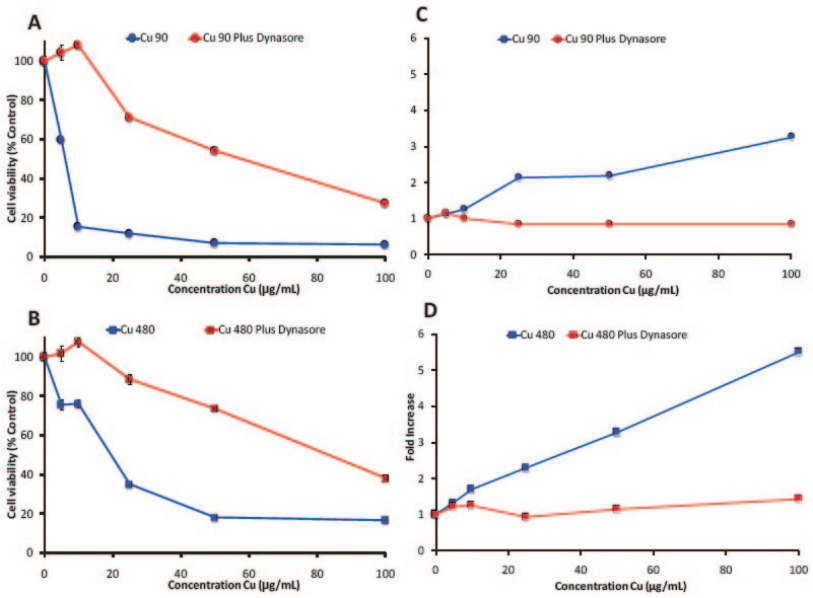

Fig. 2. – Rescue of cell viability and quenching of ROS after 25 μM Dynasore pretreatment for 1 h. (A-B) Cell viability assessment and (C-D) Cellular ROS production (Red = with 25 μM Dynasore, Blue = without Dynasore). Note that viability is significantly increased at all concentrations with 25 μM Dynasore pretreatment for 1 h for both (A) Cu 90 and (B) Cu 480 NPs (paired t-test one-tailed, $p < 0.05$). Similarly, ROS production is significantly reduced after pretreatment with 25 μM Dynasore for both (C) Cu 90 and (D) Cu 480 NPs (paired t-test one-tailed, $p < 0.05$).

to the Cu 90, which appeared to be more fused and agglomerated. The metallic composition of these two samples was confirmed with powder X-ray diffraction (XRD): both spectra revealed minimal surface oxidation on the Cu NPs (fig. 1C-D).

In accordance with previous studies that expound on the cytotoxicity of Cu NPs *in vitro* [23-26], both sizes of Cu NP yielded cell viability values of less than 50% at concentrations ranging from 25–100 μg/mL following 3 h exposures as measured with MTS (fig. 2A-B). This cytotoxicity was greater for Cu 90 (fig. 2A) compared to Cu 480 (fig. 2B), with a steeper drop in viability at the lower concentrations. Similarly, the production of reactive oxygen species (ROS) increased in a dose-dependent manner at the same concentrations and exposure end points (fig. 2C-D). However, pre-incubation of the cells for 1 h with the endocytosis inhibitor Dynasore followed by 3 h of exposure to NPs significantly reduced the cytotoxic effects of both sizes of Cu NPs (fig. 2A-B) and quenched ROS generation (fig. 2C-D). These beneficial effects were not evident with co-incubation when Dynasore and the NPs were applied to the cells at the same time.

These results indicate that Dynasore pretreatment is necessary for bio-modulation and the rescue effect, which is consistent with other similar studies [4, 7-11].

Because Dynasore has been primarily used for its function as an endocytosis inhibitor, it would seem that the observed cytotoxicity modulation by Dynasore pretreatment is due, at least in part, to blockage of Cu NP internalization. However, as a chemical inhibitor, Dynasore may possess other secondary effects that are unreported to date. For example, Dynasore may be reducing toxicity through other mechanisms. Therefore, we sought to confirm visible alterations in uptake with transmission electron microscopy

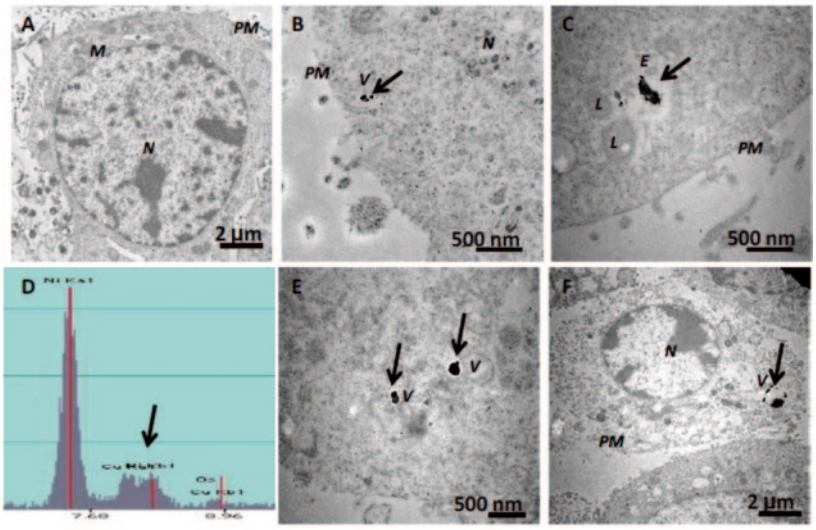

Sample	Cu Uptake (µg/ml)	Cu Uptake (+Dynasore)
Cu 90	12.8 ± 3.5	13.5 ± 4.9
Cu 480	23.2 ± 11.9	21.4 ± 4.4
$CuCl_2$	N/A	N/A

Fig. 3. – Selected TEM micrographs, representative EDXS spectra demonstrating low Cu NP uptake and localization inside cells with or without 25 μM Dynasore pretreatment for 1 h and quantification of low uptake with AAS. (A) Control, (B) Cu 90, (C) Cu 480, (D) Representative EDXS: Large Ni signal from TEM grid, representative Cu signal (black arrow) from Cu NP identified inside cell and background Os signal from cell staining procedure, (E) Cu 90 plus 25 μM Dynasore pretreatment for 1 h, (F) Cu 480 plus 25 μM Dynasore pretreatment for 1 h. Note that the uptake of Cu NPs was very low under both treatment conditions. Associated table containing AAS data demonstrates no quantifiable differences in Cu uptake with or without Dynasore pretreatment. Abbreviations: PM: plasma membrane, N: nucleus, M: mitochondria, V: vacuole, E: endosome, L: lysosome. Black arrows denote intracellular Cu NPs.

(TEM) and assess quantifiable changes in the amount of internalized Cu with atomic absorption spectroscopy (AAS). High resolution TEM has been previously used to track various NPs inside individual cells [27, 28, 12] and can be used in conjunction with energy-dispersive X-ray spectroscopy (EDXS) to provide morphological and elemental verification of the NPs [22]. In this case, we found very low internalization of both sizes of Cu NPs with and without short-term inhibition of endocytosis after evaluation of over 100 cells from each sample (fig. 3). Nonetheless, the Cu NPs that did enter cells were localized to intracellular vacuoles (V), such as endosomes and lysosomes, confirming the transient effects of a pretreatment blocking methodology. Quantification with AAS corroborates minimal differences in uptake for cells pretreated with Dynasore (fig. 3, associated table). Therefore, uptake inhibition does not seem to be the mechanism at work reducing cytotoxicity.

Other potential interactions of Dynasore with the Cu NPs such as alterations in fundamental aggregation behavior and surface interaction of Cu NPs under biological conditions were examined in order to more firmly establish a relationship between effects on physicochemical properties and the observed cytotoxicity rescue (fig. 4). Changes in size after dispersion in cell culture media is caused by transient clustering of the

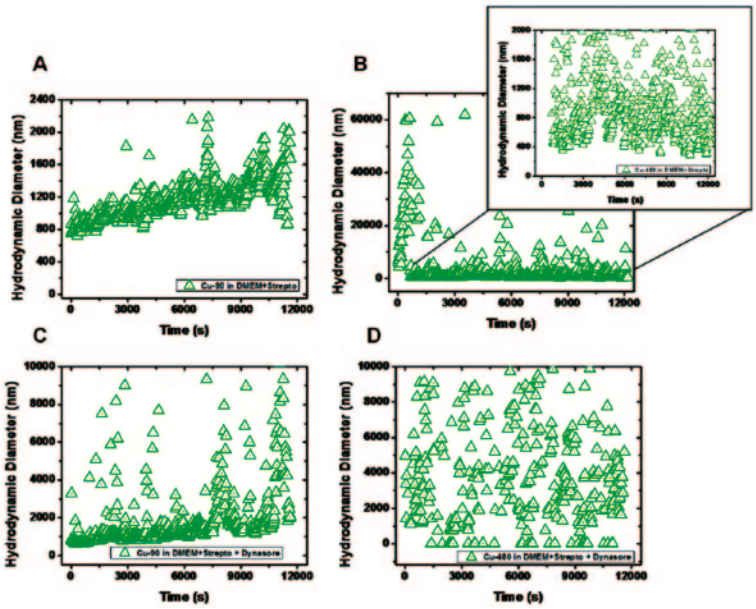

Fig. 4. – Time-dependent aggregation behavior of Cu NPs under cell culture conditions (37 °C, 0–3 h). (A) Cu 90 NPs and (B) Cu 480 NPs, (C) Cu 90 NPs+25 μM Dynasore and (D) Cu 480 NPs+25 μM Dynasore. Inset in (B) is enlargement of lower condensed values. All values presented are average hydrodynamic diameters of the particle suspension at respective time point. Note that the addition of Dynasore increases the size distribution of both Cu NP samples (C-D).

NPs, which may directly affect the NP's chemical properties and/or limit cellular uptake by normal mechanisms such as clathrin-dependent endocytosis. In conventional uptake mechanisms, the upper threshold of internalization size is typically limited to ~ 500 nm. Changes in aggregation after addition of Dynasore may reflect a change in physicochemical properties, which may affect potential for cytotoxicity. We examined the aggregation behavior of the two different sizes of Cu NPs (90 nm and 480 nm) with and without the addition of Dynasore over a 3 h period at 37 °C in biological exposure conditions with time-resolved dynamic light scattering [18, 29].

The Cu NP colloidal stability analysis demonstrated that the smaller Cu 90 NPs (fig. 4A) had a slower increase in size over time with less variability in their average size compared to their larger Cu 480 NP counterpart (fig. 4B). The Cu 480 NPs aggregated soon after addition to the exposure medium and continued to demonstrate large variability in particle aggregate size throughout the exposure time period. Furthermore, the Cu 90 NPs continued to increase in size over the duration of the experiments, yet remained smaller in hydrodynamic diameter compared to the Cu 480 NPs; confirming a true size difference for the two Cu NPs under biological conditions. In agreement, the primary size and size distributions obtained with HRTEM ranged from 40–170 nm for the Cu 90 NPs and 100–1000 nm for the Cu 480 NPs (fig. 1A-B), where the Cu 480 NPs showed a wider size distribution compared to the Cu 90 NPs. Both suspensions demonstrated the presence of much larger agglomerate sizes compared to the primary size of the Cu NPs, suggesting that the cells are exposed to a variety of aggregates sizes for both samples. Similar results were obtained with traditional DLS (data not shown). Interestingly, the addition of the chemical Dynasore resulted in the formation of Cu NP networks, which were more widely distributed in their size. For example, both the Cu 90 and Cu 480 with

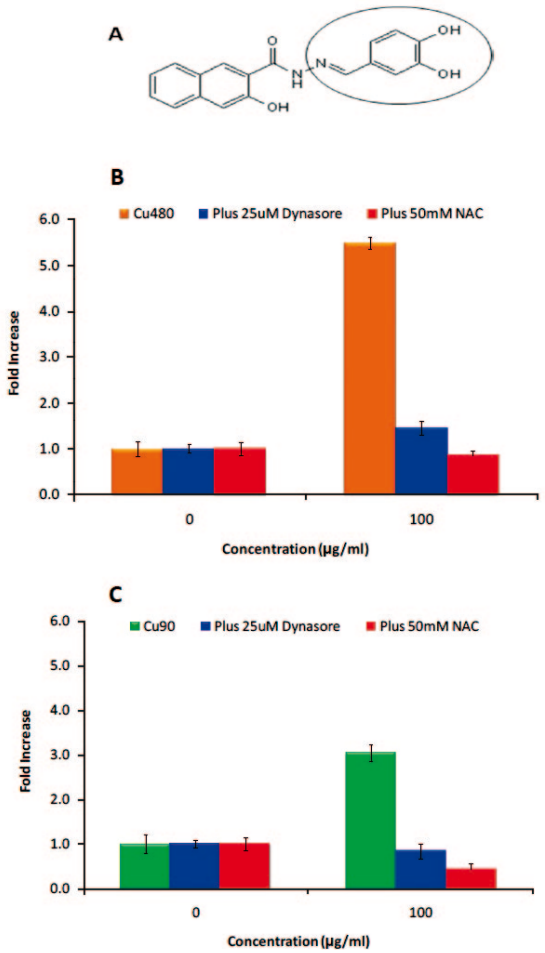

Fig. 5. – Proposed potential mechanism of Dynasore cytotoxicity rescue ROS quenching with reactive phenolic hydroxyl end groups as free radical chain reaction terminators. (A) Dynasore chemical structure with reactive end groups circled. (B) Comparison of ROS quenching ability of Dynasore to known ROS-quencher NAC in Cu 90. (C) Comparison of ROS quenching ability of Dynasore to known ROS-quencher NAC in Cu 480. In both cases, it appears that Dynasore functions similarly to NAC to significantly reduce ROS levels.

Dynasore formed aggregates with sizes up to 10 μm (fig. 4C-D). In general, it appears that addition of Dynasore increased network formation, which caused reduced toxicity of the Cu NP samples independent of their initial primary size. For example, the overall dispersion trends follow the cell viability trends: Cu 480/Dynasore > Cu 90/Dynasore > Cu 480 > Cu 90 (fig. 2). These networks may be related to ions from the media bridging the OH- groups that exist within the Dynasore molecules and contribute to the reduction of cytotoxicity observed in this way.

However, Dynasore may affect not only the physical properties of the Cu NPs but also their chemical reactivity. While we originally hypothesized that ROS reduction may be caused by blocking uptake (fig. 2C-D), Dynasore may instead be acting as an ROS quencher, leading to increased cell viability. Dynasore can potentially act as a free radical scavenger because of the three hydroxyl groups in its chemical structure (fig. 5A).

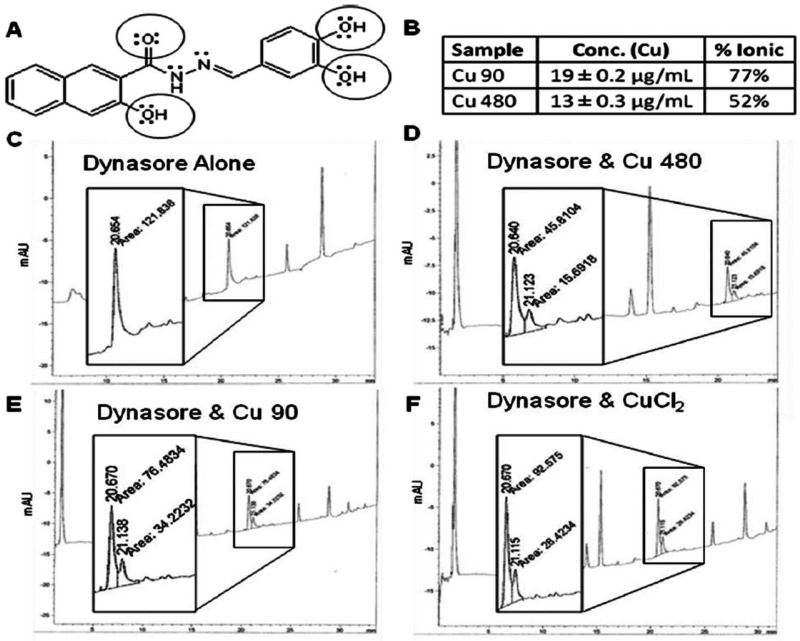

Fig. 6. – Potential mechanism of Dynasore cytotoxicity rescue through Cu^{2+} chelating by 5- or 6-membered rings. (A) Dynasore chemical structure with lone pairs that can chelate Cu ions indicated. (B) Significant amount of dissolution and release of Cu ions for both Cu 90 and Cu 480. (C) Corroboration of potential Cu^{+2} ion chelation with HPLC; similar splitting of the Dynasore peak after addition of (D) Cu 480, (E) Cu 90, and (F) $CuCl_2$, indicates a change in electronic structure. Inset images are enlargements of the chemical peaks of interest.

In this case, free radicals generated at the surface of the Cu NPs [30] may be scavenged by Dynasore under biological conditions by abstracting a hydrogen atom from one of the ortho-phenolic hydroxyl groups of Dynasore, thereby inactivating the radical species responsible for cellular damage. In support of this, we found that Cu NP-induced reactive oxygen species (ROS) in an acellular environment was significantly quenched after the addition of Dynasore (data not shown). To further confirm this potential mechanism, we tested a known ROS quencher, N-acetyl-cysteine (NAC). As expected, there was a significant quenching of ROS upon pre-incubation with 50 mM NAC for 1 h prior to exposure to 100 μg/mL of Cu 90 or Cu 480 NPs (fig. 5B-C). The similar type of ROS reduction with both NAC and Dynasore corroborate this ROS quenching as a potential mechanism of cytotoxicity modulation.

Another possible mechanism for the apparent rescue effect of Dynasore may be related to its complexing with Cu ions released by the Cu NPs, thereby reducing the concentration of free Cu ions in the media and their availability to induce damaging effects to the cells (fig. 6). It is well known that copper NPs generate ROS and cytotoxicity that is linked to dissolution and ionic release [31-35]. Removal of metallic ions from the cellular environment through chelation has been used to alleviate conditions involving toxic levels of metallic ions such as Wilson's disease [36, 37]. In this case, Dynasore's polyphenolic structure may allow for Cu^{+2} ion chelation by forming 5- or 6-membered rings. Some antioxidants with similar polyphenolic structural features, such as the flavornoids

rutin and quercetin, were reported to behave via similar mechanisms [38]. Recently, additional phenolic compounds have demonstrated specific antioxidant reactivity towards hydrogen peroxide and copper ions [39]. Through tangential flow filtration, we found that both of the Cu NP samples produced significant concentrations of ions under cell culture conditions (fig. 6B). The toxicity of these Cu ions alone was corroborated by the finding that comparable amount of Cu^{+2} ions from $CuCl_2$ were also highly toxic (data not shown).

To corroborate this potential mechanism via ion chelation, we performed high-performance liquid chromatography to characterize electronic configuration. Our spectrographs show a clear peak for the Dynasore molecule at roughly 20.64–20.67 min (data not shown). In addition, the peak for the Dynasore molecule through HPLC was split after the addition of Cu 90, Cu 480, and $CuCl_2$ (fig. 6C-F), indicating a change in electronic configuration that may be related to the ion chelation. This splitting is not based on the mere presence of any chemical species in the media nor the particles themselves, since none of these samples by themselves have a peak near this region. The similar peak splitting for both particles that release ions and pure ions suggests that similar chelation mechanisms may be occurring in all three cases. Therefore, it is possible that Dynasore may form complexes with the Cu ions to reduce their bio-availability and toxic potential. These complexes may be related to the networks observed through time-resolved DLS (fig. 4C-D).

4. – Conclusions

In summary, we provide evidence that Dynasore reduces the cytotoxicity of Cu NPs, but not through uptake inhibition. Instead, Dynasore's ability to rescue cells from Cu NP-induced toxicity is based on other secondary effects. We have proposed and provided evidence to support three possible mechanisms that are independent of the Cu NP size or form: physical alterations in aggregation (fig. 4), chemical ROS quenching (fig. 5), and chemical ion chelation (fig. 6). Furthermore, the cell viability rescue effect of Dynasore also extends to the soluble form of copper in $CuCl_2$. All in all, our results suggest that some of the beneficial effects previously observed during Dynasore treatment strategies [11] may be due, in part, to the physicochemical alterations brought forth in this work. Nonetheless, pretreatment with Dynasore for 1 h is not sufficient to fully recover cell viability to control levels after 3 h of continuous exposure to Cu NP concentrations exceeding 10 μg/mL. This indicates that high doses of Cu NPs may overwhelm the short-term protective effects of Dynasore leading to alternative mechanisms of Cu NP-induced cell death. Cumulatively, our results aid in mechanistically explaining nanomaterial interactions with biological species at the cellular level. These results have far-reaching implications for understanding the complex interactions that occur with NPs in biological environments, especially during mechanistic chemical modification strategies.

* * *

AMS received funding from the Joint Science and Technology Office for Chemical and Biological Defense (JSTO-CBD), a program administered by the Defense Threat Reduction Agency (DTRA). JBL was sponsored by the Student Temporary Employment Program (STEP) at AFRL/RHPB. Special thanks to Ms. Beth Maurer (AFRL/RHPB), Cadets Michelle Kiyota and Catherine Kiyota (USAFA), Dr. Latha Narayanan (AFRL/RHC), and Dr. William Steinecker (IDCAST) for technical assistance. AFRL Clearance #96ABW-2012-0390.

REFERENCES

[1] Cioffi N., Torsi L., Ditaranto N., Tantillo G., Ghibelli L., Sabbatini L., Bleve-Zacheo T., D'Alessio M., Zambonin P. G. and Traversa E., *Chem. Mater.*, **17** (2005) 5255.
[2] Anyaogu K. C., Fedorov A. V. and Neckers D. C., *Langmuir*, **24** (2008) 4340.
[3] Schrand A. M., Rahman M. F., Hussain S. M., Schlager J. J., Smith D. A. and Syed A. F., *WIREs Nanomed. Nanobiotechnol.*, **2** (2010) 544.
[4] Macia E., Ehrlich M., Massol R., Boucrot E., Brunner C. and Kirchhausen T., *Dev. Cell*, **10** (2006) 839.
[5] Kirchhausen T., Macia E. and Pelish H. E., *Methods Enzymol.*, **438** (2008) 77.
[6] Thompson H. M. and McNiven M. A., *Nat. Chem. Biol.*, **2** (2006) 355.
[7] Newton A. J., Kirchhausen T. and Murthy V. N., *Proc. Natl. Acad. Sci. U.S.A.*, **103** (2006) 17955.
[8] Martinez-Argudo I. and Jepson M. A., *Microbiology*, **154** (2008) 3887.
[9] Gratton S. E. A., Ropp P. A., Pohlhaus P. D., Luft J. C., Madden V. J., Napier M. E. and DeSimone J. M., *Proc. Natl. Acad. Sci. U.S.A.*, **105** (2008) 11613.
[10] Jiang X., Dausend J., Hafner M., Musyanovych A., Rocker C., Landfester K., Mailander V. and Nienhaus G. U., *Biomacromolecules*, **11** (2010) 748.
[11] Soriano J., Stockert J. C., Villanueva A. and Canete M., *Histochem. Cell Bio.*, **133** (2010) 449.
[12] Schrand A. M., Lin J. B., Ciftan Hens S. and Hussain S. M., *Nanoscale*, **3** (2011) 435.
[13] Jiang X., Röcker C., Hafner M., Brandholt S., Dörlich R. M. and Nienhaus G. U., *ACS Nano*, **4** (2010) 6787.
[14] Fazlollahi F., Angelow S., Yacobi N. R., Marchelletta R., Yu A. S., Hamm-Alvarez S. F., Borok Z., Kim K. J. and Crandall E. D., *Nanomedicine*, **7** (2011) 588.
[15] Lunov O., Syrovets T., Loos C., Beil J., Delacher M., Tron K., Nienhaus G. U., Musyanovych A., Mailänder V., Landfester K. and Simmet T., *ACS Nano*, **5** (2011) 1657.
[16] Murdock R. C., Braydich-Stolle L., Schrand A. M., Schlager J. J. and Hussain S. M., *Toxicol. Sci.*, **101** (2007) 239.
[17] Surdo E. M., Khan I. A., Choudhury A. A., Saleh N. B. and Arnold W. A., *J. Haz. Mat.*, **188** (2011) 334.
[18] Saleh N. B., Pfefferle L. D. and Elimelech M., *Environ. Sci. Technol.*, **42** (2008) 7963.
[19] Braydich-Stolle L. K., Schaeublin N. M., Murdock R. C., Jiang J., Biswas P., Schlager J. J. and Hussain S. M., *J. Nanopart. Res.*, **11** (2009) 1361.
[20] Wang H. and Joseph J. A., *Free Radic. Biol. Med.*, **27** (1999) 612.
[21] Hussain S. M. and Frazier J. M., *Toxicol. Sci.*, **69** (2002) 424.
[22] Schrand A. M., Schlager J. J., Dai L. and Hussain S. M., *Nat. Protoc.*, **5** (2010) 744.
[23] Midander K., Cronholm P., Karlsson H. L., Elihn K., Möller L., Leygraf C. and Wallinder I. O., *Small*, **5** (2009) 389.
[24] Lanone S. *et al. Part. Fibre Toxicol.*, **6** (2009) 14.
[25] Fahmy B. and Cormier S. A., *Toxicol. In Vitro*, **23** (2009) 1365.
[26] Karlsson H. L., Gustafsson J., Cronholm P. and Möller L., *Toxicol. Lett.*, **188** (2009) 112.
[27] Schrand A. M., Huang H., Carlson C., Schlager J. J., Osawa E., Hussain S. M. and Dai L., *J. Phys. Chem. B.*, **111** (2007) 2.
[28] Schrand A. M., Braydich-Stolle L. K., Schlager J. J., Dai L. and Hussain S. M., *Nanotechnology*, **19** (2008) 1.
[29] Saleh N. B., Pfefferle L. D. and Elimelech M., *Environ. Sci. Technol.*, **44** (2010) 2412.

[30] Nel A., Xia T., Mädler L. and Li N., *Science*, **311** (2006) 622.
[31] Griffitt R. J., Weil R., Hyndman K. A., Denslow N. D., Powers K., Taylor D. and Barber D. S., *Environ. Sci. Technol.*, **41** (2007) 8178.
[32] Kasemets K., Ivask A., Dubourguier H. C. and Kahru A., *Toxicol. In Vitro*, **23** (2009) 1116.
[33] Heinlaan M., Ivask A., Blinova I., Dubourguier H. C. and Kahru A., *Chemosphere*, **71** (2008) 1308.
[34] Meng H., Chen Z., Xing G., Yuan H., Chen C., Zhao F., Zhang C., Wang Y. and Zhao Y., *J. Radioanal. Nucl. Ch.*, **272** (2007) 595.
[35] Meng H., Chen Z., Xing G., Yuan H., Chen C., Zhao F., Zhang C. and Zhao Y., *Toxicol. Lett.*, **175** (2007) 102.
[36] Thompson K. H. and Orvig C., *Science*, **300** (2003) 936.
[37] Subramanian I., Vanek Z. F. and Bronstein J. M., *Curr. Neurol. Neurosci. Rep.*, **2** (2002) 317.
[38] Afanas'ev I. G., Dorozhko A. I., Brodskii A. V., Kostyuk V. A. and Potapovitch A. I., *Biochem. Pharmacol.*, **38** (1989) 1763.
[39] Labieniec M. and Gabryelak T., *Cell Biol. Int.*, **30** (2006) 761.